Title
NUCLEAR EXCITATION OF Al, Si, Ca AND Co PRODUCED BY u- CAPTURE

Authors
Temple, L.E.
Kaplan, S.N.
Pyle, R.V.
et al.

Publication Date
1971-12-01

Presented at the Muon Physics Conference
Ft. Collins, Colorado, September 6-9, 1971

LBL 24 c.2
Preprint

NUCLEAR EXCITATION OF Al, Si, Ca and Co PRODUCED BY μ^- CAPTURE

L. E. Temple, S. N. Kaplan, R. V. Pyle, and G. F. Valby

December 1971

AEC Contract No. W-7405-eng-48

DISCLAIMER

NUCLEAR EXCITATION OF Al, Si, Ca and Co PRODUCED BY μ^- CAPTURE*†

L. E. Temple, S. N. Kaplan, R. V. Pyle, and G. F. Valby

December 1971

Lawrence Berkeley Laboratory
University of California
Berkeley, California 94720

ABSTRACT

De-excitation gamma rays from residual nuclei following μ^- capture in natural Al, Si, Ca, and Co targets were observed. The results are consistent with neutron emission data and previously reported gamma transition measurements. The identified gamma transitions account for 81, 42, 42, and 71% of the nuclear muon captures respectively in Al, Si, Ca, and Co. Charged-particle emission is observed 14% of the time in Ca, 10% of the time in Si, and not at all in Al and Co. Levels corresponding to an excitation energy of 27 MeV above the ground state in ^{59}Co and more than 20 MeV above the ground state in the other targets were observed. Levels populated in the $^{40}Ca(\mu^-,\nu n)^{39}K$ reaction correlate closely with those observed in the $^{40}Ca(\gamma,p\gamma')^{39}K$ photo-excitation reaction. Comparison of the Si target results with the photo-excitation and electro-excitation reactions on ^{28}Si suggest the presence of a giant magnetic resonance in muon capture.

---

† Paper presented by L. E. Temple at the Muon Physics Conference, Fort Collins, Colorado, September 6 - 10, 1971.

METHOD

The pulse output of a 15-cc Ge(Li) detector was put in coincidence with one of four time gates, converted to a digital signal, and stored in one of four 4096-channel pulse-height spectra on an M6 Data Disc via a buffer in the core of a PDP-5 computer. The Ge(Li) prompt pulse was delayed with respect to the counter telescope muon-stop trigger to allow the accumulation of a "negative-time" spectrum corresponding to photons uncorrelated with a stopping muon (G1). Mu-mesic x rays and prompt gamma rays occurring within a 50-nsec band about a muon stop were recorded in a second spectrum (G2). Two additional spectra corresponding to photons detected in two sequential time intervals following a muon stop were taken (G3, G4). The time relationship of the muon-stop trigger pulse and the four routing gates with a Ge(Li) signal is shown in Fig. 1. The Ge(Li) pulses γ_1, γ_2, γ_3, and γ_4 are stored respectively in the negative-time, prompt-time, short-delay, and long-delay spectra. Figure 2 shows the first 1600 channels of the data accumulated in fours for the Ca target. The Ca mu-mesic K x-ray series is evident in G2. The positron annihilation line at 511 keV; the $^{10}B(n, \alpha)^{7}Li$ line at 478 keV; and the peak due to inelastic neutron scattering in the Ge(Li) detector, $^{72}Ge(n,n')^{72}Ge$, are samples of background and are labeled on the G1 spectrum. To varying degrees both the x rays and these background lines occur in G3 and G4. Gamma-ray peaks at energies corresponding to nuclear transitions in ^{39}K, ^{39}Ar, and ^{38}Ar have been identified in G3 and appear less intensely in G4.

Recording of the prompt spectrum for Al, Si, Ca, Fe, Co, Ni, Cu, Mo, Ag, Sn, and Pb targets in the same experimental configuration under which the nuclear gamma-ray data was taken provided data for an absolute detector efficiency determination. Corrections for the muon stopping distribution, target-detector geometry, and photon attenuation in the target were made in the efficiency calculations. It was assumed that each stopping muon produced a K x ray.

Ratios of K_α x rays to the sum of all K x rays were determined for the Al, Si, Ca, Fe, Co, Ni, Cu, and Mo targets. This ratio was assumed to be approximately 0.9 for the Ag, Sn, and Pb targets. The full-energy-peak (FEP) absolute efficiency obtained in this manner covered an energy range from 345 to 5960 keV and was close to an exponential up to 3950 keV.

To extend the energy range and determine the response shape in more detail, an FEP relative efficiency curve with measurements at 37 energies from 59 to 4072 keV was made by using IAEA standard sources and other radioisotopes. This curve was then scaled to the effective target efficiency at the K_α x ray for the target; i.e., target geometry and muon stopping distribution corrections were not made, and a target attenuation correction was then made as a function of energy. A relative double-escape-peak (DEP) efficiency curve was scaled to the absolute DEP efficiency at the Mo K_α x-ray energy and plotted with the absolute DEP efficiencies measured with the Ag, Sn, and Pb targets. A best fit of the DEP efficiency response for a 15-cc planar detector as calculated by Euler and Kaplan[1] was made to these points. Self-attenuation corrections as a function of energy were then made for each target.

Energy calibrations were taken frequently during the experiment, using ^{60}Co and ^{24}Na sources and the ^{16}O γ rays from the β decay of ^{16}N formed in the reaction ^{16}O(n,p)^{16}N on the cyclotron platform. Agreement of energy assignments for well-known gamma transitions in our data indicate an uncertainty of less than 1 keV over the total energy range, which extended from about 250 to 6500 keV.

A plot of the experimental sensitivity vs γ-ray energy for sharp peaks and Doppler-broadened peaks is shown in Fig. 3. Doppler broadening of a peak occurs when the lifetime τ_m of the level from which the transition occurs is short compared with the time required for the nucleus to slow down following the recoil from the neutrino or a neutrino plus neutron. This time is of the order of 10^{-12} to 10^{-13}sec. Such Doppler-broadened peaks, as previously described for O,[2] are clearly evident in the spectra from both the Ca and Si tragets. Figure 4 depicts the broad peaks in the Ca data at 5.28, 5.62, 5.96, and 6.35 MeV. All of these peaks are identified as transitions in ^{39}K.

RESULTS

A nuclear level diagram showing schematically the intensities and identifications of observed peaks in the summed G3 and G4 spectra for the Al target is shown in Fig. 5. Transitions from levels corresponding to residual excitations, as high as 22 MeV above the ^{27}Al ground state, are observed in ^{25}Mg. No transitions implying proton emission were observed. The ^{26}Mg 1809-keV transition was quite intense. Table I displays the same information in tabular form as well as entries for the number of times a level is populated and the number of times each isotope is formed per 100 nuclear captures. Seventy percent of the time a muon is captured in ^{27}Al an excited state in ^{26}Mg is produced, while excited states in ^{25}Mg and ^{27}Mg are observed 7% and 5% of the time respectively. These values constitute lower limits for production of these final states. As was shown in Kaplan's talk[3] these results are in good agreement with the neutron multiplicities determined by MacDonald et al.[4]

The level diagram for the Co target is shown in Fig. 6. Here the

E_γ = 1322.3 keV transition identified as ^{58}Fe 2133.4-keV $3^+ \rightarrow$ 810.5-keV 2^+ is consistent also with ^{56}Mn 1321 $\rightarrow$ 0. However, the branching to the 1674.1 level is consistent with the current assignment. Although the Nuclear Data Sheets[5] show no branch of the ^{57}Fe 1265-keV state to the ground state, it is here identified as such, based on Groshev's[6] work. He shows the line twice, once as 1265 $\rightarrow$ 0 and once as 1627 $\rightarrow$ 366.8. The total yield of the 366.8 $\rightarrow$ 14.4 transition is only 0.9$\pm$0.1, whereas the E_γ = 1265 intensity is approximately 11%, indicating that most of the observed E_γ = 1265 intensity is not accounted for in this manner. The Co results are shown in Table II and compared with transition intensities measured by Backenstoss[7] et al. Yields for the 4550- and 1674-keV levels in ^{58}Fe are consistent with at most only 0.3 of the 4.5% yield of the E_γ = 1674.1 keV gamma being due to the 4550 $\rightarrow$ 2876 transition. Agreement between the two experiments is very good with the single exception that Backenstoss reports a 1.4% yield to the first excited state in ^{55}Fe, which is not seen here. Such a final state requires the emission of four neutrons and is at an excitation energy 37 MeV above the ground state of ^{59}Co. We should have easily observed a yield this large. The observed transitions show no proton emission, 1.7% no-nucleon emission, 46% single-neutron emission, 18% emission of two neutrons, 5.4% emission of three neutrons, and account for 71% of the muon captures in Co.

Observed transitions in Ca are shown in Fig. 7. All transitions in ^{39}K, except the two highest energy levels, were reported earlier by Igo-Kemenes[8] et al. There are some differences between the results of this experiment and those of Igo-Kemenes et al. for excitations in ^{39}Ar. The identifications in this work are made on the basis of the energy levels and branching ratios given by Bass and Saleh-Bass.[9] The 3935-

keV level is shown dotted in ^{39}K and E_γ = 3935 keV assignment was taken as ^{38}Ar, since a 1% population of the 3935-keV level in ^{39}K would imply approximately 0.2% yields for transitions with energies of 332 and 1118 keV respectively, which were not seen. Table III contains the results for the Ca target and shows Igo-Kemenes' results for comparison. Figure 8 compares the results of three experimental methods for exciting levels in ^{39}K. The photo-excitation analog to the muon capture reaction $^{40}Ca(\mu^-,\nu n)^{39}K$ is $^{40}Ca(\gamma,p\gamma')^{39}K$. The results of Ullrich and Krauth[10] are shown for this reaction. Hinds and Middleton[11] studied the $^{40}Ca(t,\alpha)^{39}K$ reaction and conclude that the 5.28-, 5.62-, and 6.35-MeV levels in ^{39}K contain most of the $1d_{5/2}$ proton hole strength. This comparison is made to demonstrate that levels which have a shell-model type structure are populated preferentially following both muon capture and photo-excitation and to show the strong correlation between levels excited in muon capture and photo-excitation.

The nuclear level diagram for the Si target is shown in Fig. 9. There are some ambiguities in the identification of some of the peaks in the spectrum from this target. First, the E_γ = 985.7 keV transition identified as ^{28}Al 1014.5 → 30.62 is consistent with a transition in ^{27}Mg from the first excited state--984 keV, $J^\pi = 3/2^+$--to the ground state. It was assumed (possibly erroneously) that single-proton emission is unlikely, and the full intensity is ascribed to ^{28}Al. [Ascribing this peak to ^{28}Al is based on the known large transition rate to ^{28}Al (Ref. 12) and the assumed small likelihood of proton emission producing ^{27}Mg. Since there is independent evidence for single-proton emission from μ^- capture in Ca this assumption may have been unwarranted.] Second, the E_γ = 1015.1 keV transition in ^{28}Al is at the same energy as the transition from the second excited state to ground in

^{27}Al. Based on branching of the ^{28}Al 1014 level 58% to the 31-keV first excited state and 42% to the ground state, the portion of the E_γ = 1014 keV intensity assigned to ^{28}Al is 0.8. Third, although the E_γ = 2212 keV peak is consistent with a transition from the third excited ^{27}Al state to ground, this assignment is at odds with the charged-particle spectrum following photo-excitation in ^{28}Si measured by Cannington[13] et al. Fourth, the broad peak at 2175 keV with an intensity of 3.2$\pm$0.5% has not been assigned.

Figure 10 shows the two broad peaks at 2175 and 2212 keV in the Si target and two nearby sharp peaks for comparison. The peak at 2212 keV is at the correct energy for a transition in ^{27}Al. This level has a width measured to be 15.8$\pm$1.1 meV,[14] corresponding to a mean lifetime of 4.2×10^{-14} sec and should be Doppler-broadened. The first, second, fourth, and fifth states in ^{27}Al are populated following muon capture in ^{28}Si, and this correlates well with Cannington's results shown in Fig. 11. The complete absence of a proton group corresponding to an excitation of the third excited state in ^{27}Al is interesting. Perhaps the 2212-keV gamma transition is not from ^{27}Al.

Uberall[15] has suggested that there should be a strong M1 excitation to levels in ^{28}Al. Fagg[16] et al. have seen a giant resonance in the 180 deg electron scattering cross section in ^{28}Si at an excitation energy of 11.4 MeV (Fig. 12). When the energy level diagram is adjusted for the Coulomb displacement (Fig. 13), the analog state is at about 2.2 MeV in ^{28}Al.

The results for the Si target, with the above two transitions not included, are shown in Table IV. Pratt's[18] results are shown for comparison. A total of 42% of the muon captures are accounted for by observed and identified lines. The two unassigned broad lines near 2.2 MeV contribute another 7.8%. An appreciable amount of proton plus neutron emission is seen (approximately 9.5 %). Furthermore, with only the present definite assignments, transitions in ^{28}Al account for no-nucleon emission about 4% of the time, whereas other evidence indicates a large proportion of no-particle emission. We propose therefore, that either or both of the broad 2175 or 2212 keV transitions may be due to excitations in ^{28}Al corresponding to an M1 resonance as suggested by Uberall.

ADDENDUM

Since the conference, Dr. Claude Petitjean has forwarded us the thesis of Jean-Luc Vuilleumier,[17] which reported gammas following muon capture in ^{40}Ca and also called our attention to recent work on level schemes and branching ratios for ^{40}K. Additions or modifications to the tabulated data for Ca in Table III made since the conference and as a result of this new information are denoted by footnote c.

FOOTNOTES AND REFERENCES

*Work done under the auspices of the U. S. Atomic Energy Commission.

1. B. A. Euler and S. N. Kaplan, IEEE trans. Nucl. Sci. NS-17, 4, 81 (1970).

2. S. N. Kaplan, R. V. Pyle, L. E. Temple, and G. F. Valby, in High Energy Physics and Nuclear Structure, S. Devons editor (Plenum Press, New York, 1969) p. 163.

3. S. N. Kaplan, these proceedings.

4. B. MacDonald, J. A. Diaz, S. N. Kaplan, and R. V. Pyle, Phys. Rev. 139B, 1253 (1965).

5. Nuclear Data Sheets, B3-3, 4-105 (Academic Press, New York).

6. L. V. Groshev, A. M. Demidov, G. A. Kotelnikov, and V. N. Lutsenko, Nucl. Phys. 58, 465 (1964).

7. G. Backenstoss, S. Charalambus, H. Daniel, W. D. Hamilton, U. Lynen, Ch. von der Malsburg, G. Poelz, and H. V. Povel, Nucl. Phys. A162, 541 (1971).

8. P. Igo-Kemenes, J. P. Deutsch, D. Favart, L. Grenacs, P. Lipnik, and P. C. Macq, Phys. Letters 34B, 4, 286 (1971).

9. R. Bass and Fatma M. Saleh-Bass, Nucl. Phys. A131, 673 (1969).

10. H. Ullrich and H. Krauth, Nucl. Phys. A123, 641 (1969).

11. S. Hinds and R. Middleton, Nucl. Phys. 84, 651 (1966).

12. G. Bunatian, V. Evseev, L. Nikityuk, V. Pokrovsky, V. Ribakov, and I. Yutlandov, in High-Energy Physics and Nuclear Structure, S. Devons editor (Plenum Press, New York, 1969) p. 182.

13. P. H. Cannington, R. J. J. Stewart, G. R. Hogg, K. H. Lokan, and D. G. Sargood, Nucl. Phys. 72, 577 (1965).

14. S. J. Skorka, D. Evers, J. Hertel, J. Morgenstern, T. W. Retz-Schmidt, and H. Schmidt, Nucl. Phys. 81, 370 (1966).

15. Herbert Uberall, The Catholic University of America and U. S. Naval Research Laboratory, Washington, D. C., private communication.

16. L. W. Fagg, W. L. Bendel, E. C. Jones, Jr., and S. Numrich, Phys. Rev. 187, 4, 1378 (1969).

17. Jean-Luc Vuilleumier, thesis, Ecole polytechnique federale de Zurich, 1971 (unpublished).

18. Theodore A. E. C. Pratt, thesis, Carnegie-Mellon University, 1968 (unpublished).

FIGURE CAPTIONS

Fig. 1. Time relationship of the muon-stop pulse (trigger) and the four routing gates. The relative probability as a function of time of the observation of a μ^--capture γ ray is indicated by the decaying exponential curve. The four possible types of detected photons are shown on the bottom trace and described in the text.

Fig. 2. First 1600 channels of data accumulated in a 4-hr run with a Ca target.

Fig. 3. Detection sensitivity (90% confidence level) vs energy for Ca. A sensitivity of 0.003, for example, implies that the yield of a transition of 0.003 per nuclear muon capture will be seen above background with 90% confidence. The reduced sensitivities for peaks that are Doppler-broadened because of decay in flight are due to the greater background areas under the broader peaks. The numerical values are based on the plausible, but somewhat arbitrary, assumptions of isotropic recoils from an 80-MeV neutrino and a 3-MeV neutron.[2]

Fig. 4. Doppler-broadened peaks in Ca spectrum. The bars show the full width at half maximum (FWHM) of the detector response for a sharp line.

Fig. 5. Nuclear level diagram for ^{27}Al target showing population of states following μ^- capture.

Fig. 6. Nuclear level diagram for ^{59}Co target showing population of states following μ^- capture.

Fig. 7. Nuclear level diagram for ^{40}Ca showing population of states following μ^- capture.

Fig. 8. Comparison of $^{40}Ca(\mu^-,\nu n\gamma)^{39}K$ reaction with $^{40}Ca(\gamma,p\gamma')^{39}K$ and $^{40}Ca(t,\alpha)^{39}K$ reactions. Note the high relative yields corresponding to the $1/2^+$ neutron hole level at 2.53 MeV and the three $5/2^+$ levels near 6 MeV in all three reactions.

Fig. 9. Nuclear level diagram for ^{28}Si showing population of states following μ^- capture. The cross hatched region corresponds to the location of a possible M1 resonance in ^{28}Al.

Fig. 10. Doppler-broadened lines in Si spectrum. The bars show the FWHM of the detector response for a sharp line.

Fig. 11. Charged-particle spectrum following photo-excitation in ^{28}Si (after Cannington et al.[13]). The peaks labelled α_0 and α_1 correspond to alpha groups. Those labelled P_0, P_1, P_2, P_4 and P_{5-6} are proton groups corresponding to the ground state, first-, second-, fourth-, and fifth and sixth-excited states in ^{27}Al. Note the absence of a proton group at the arrow which corresponds to the third excited state in ^{27}Al.

Fig. 12. 180 deg electron scattering by ^{28}Si. Covers excitation energy range of 10 to 15 MeV (after Fagg et al.[16]).

Fig. 13. Nuclear level diagram adjusted for the Coulomb displacement so that ^{28}Si and ^{28}Al analog states are approximately aligned (after Fagg et al.[16]).

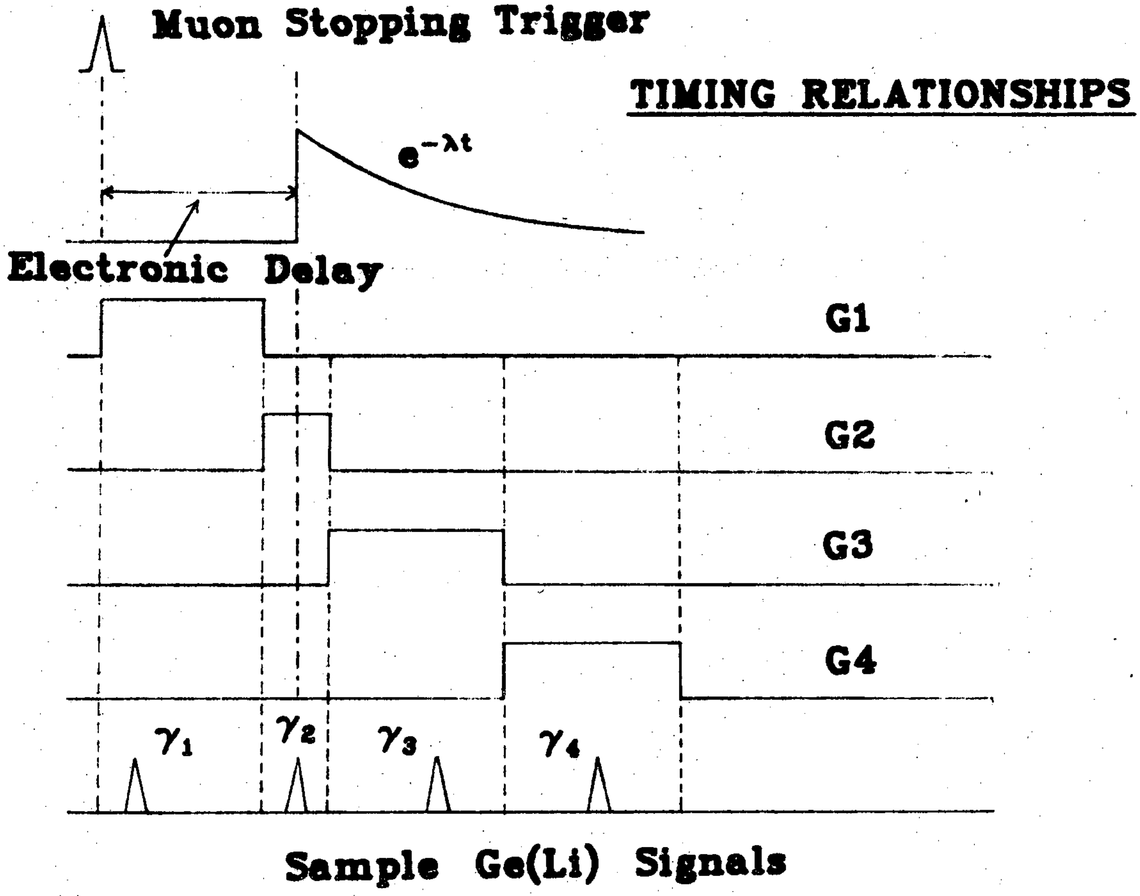

XBL 7112-1809

Fig. 1

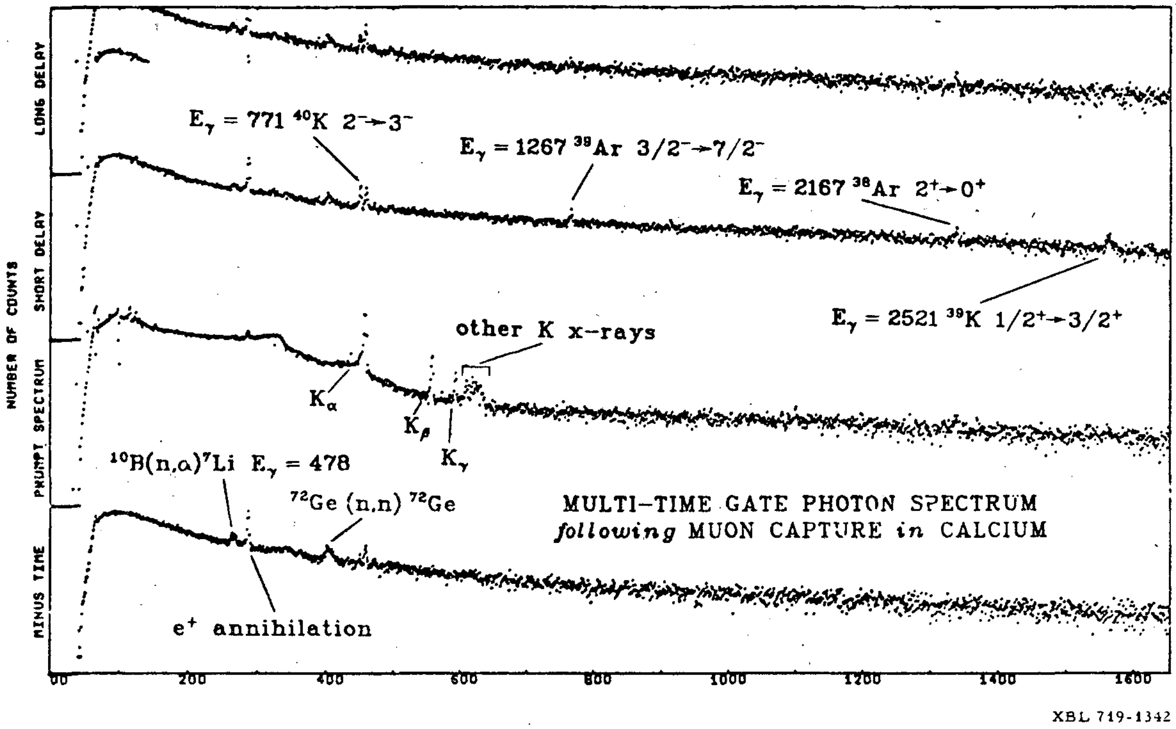

LONG DELAY
SHORT DELAY
PROMPT SPECTRUM
MINUS TIME
NUMBER OF COUNTS
E$_\gamma$ = 771 ^{40}K 2$^-$→3$^-$
E$_\gamma$ = 1267 ^{39}Ar 3/2$^-$→7/2$^-$
E$_\gamma$ = 2167 ^{38}Ar 2$^+$→0$^+$
E$_\gamma$ = 2521 ^{39}K 1/2$^+$→3/2$^+$
other K x-rays
K$_\alpha$
K$_\beta$
K$_\gamma$
^{10}B(n,α)^{7}Li E$_\gamma$ = 478
^{72}Ge (n,n) ^{72}Ge
MULTI-TIME GATE PHOTON SPECTRUM
following MUON CAPTURE in CALCIUM
e$^+$ annihilation
00
200
400
600
800
1000
1200
1400
1600
XBL 719-1342

Fig. 2

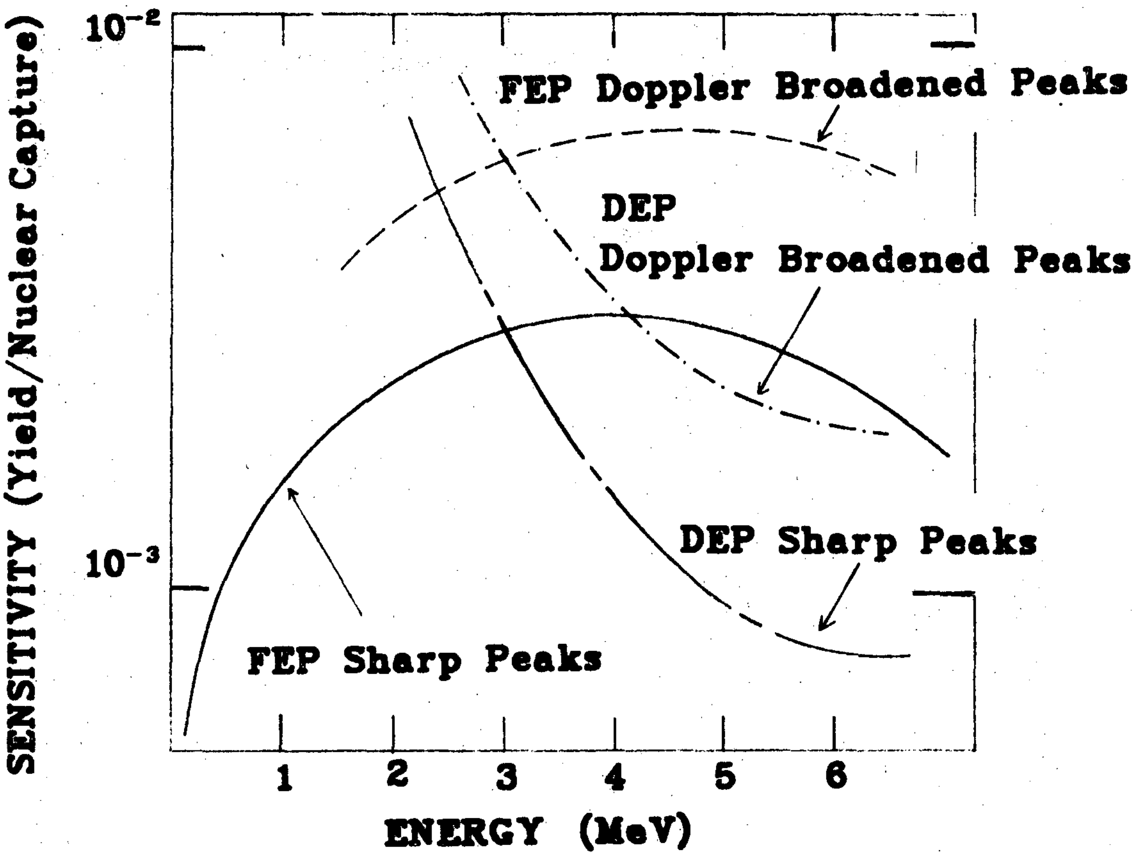

XBL 7112-1810

Fig. 3

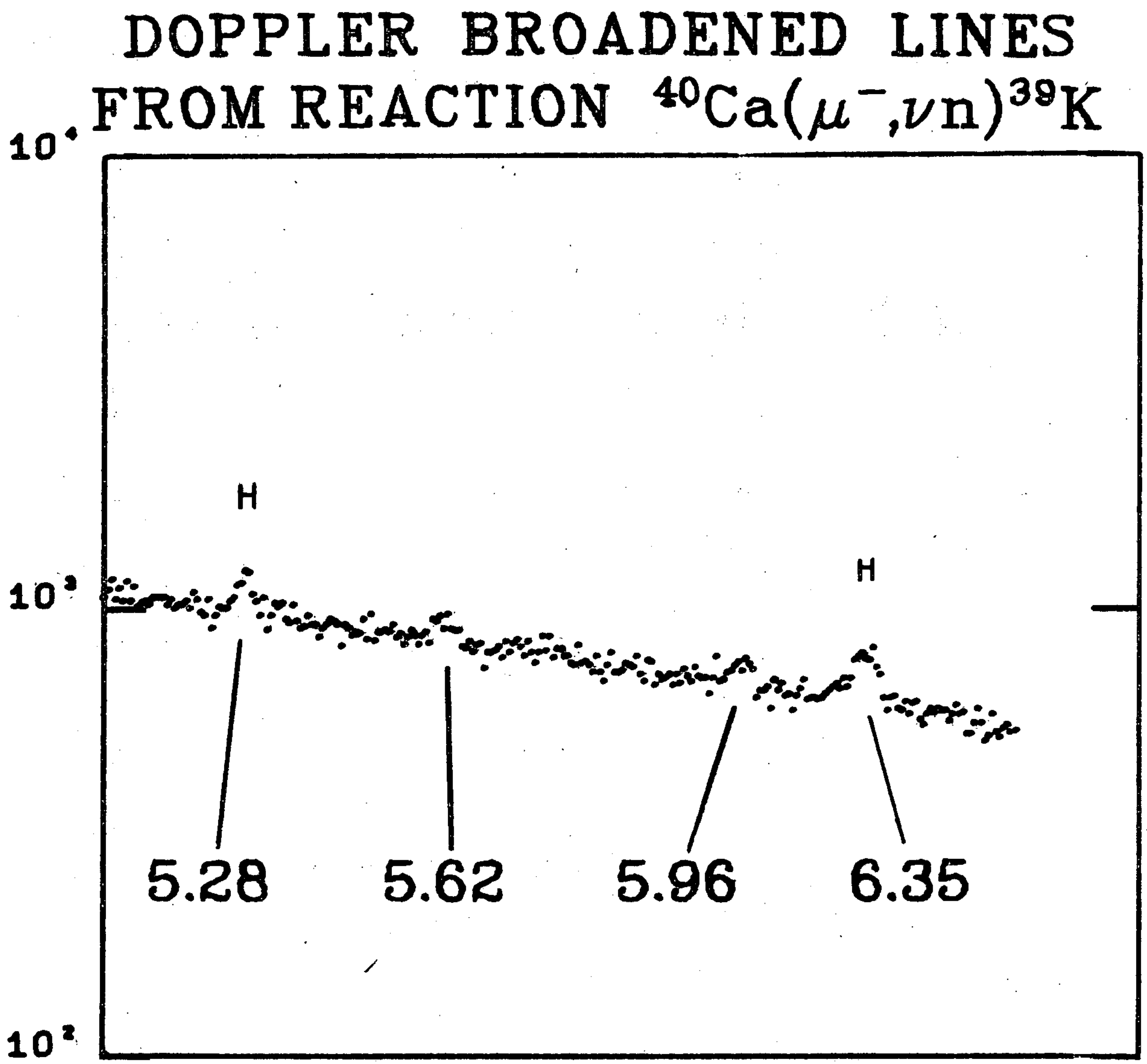

XBL 719-1340

Fig. 4

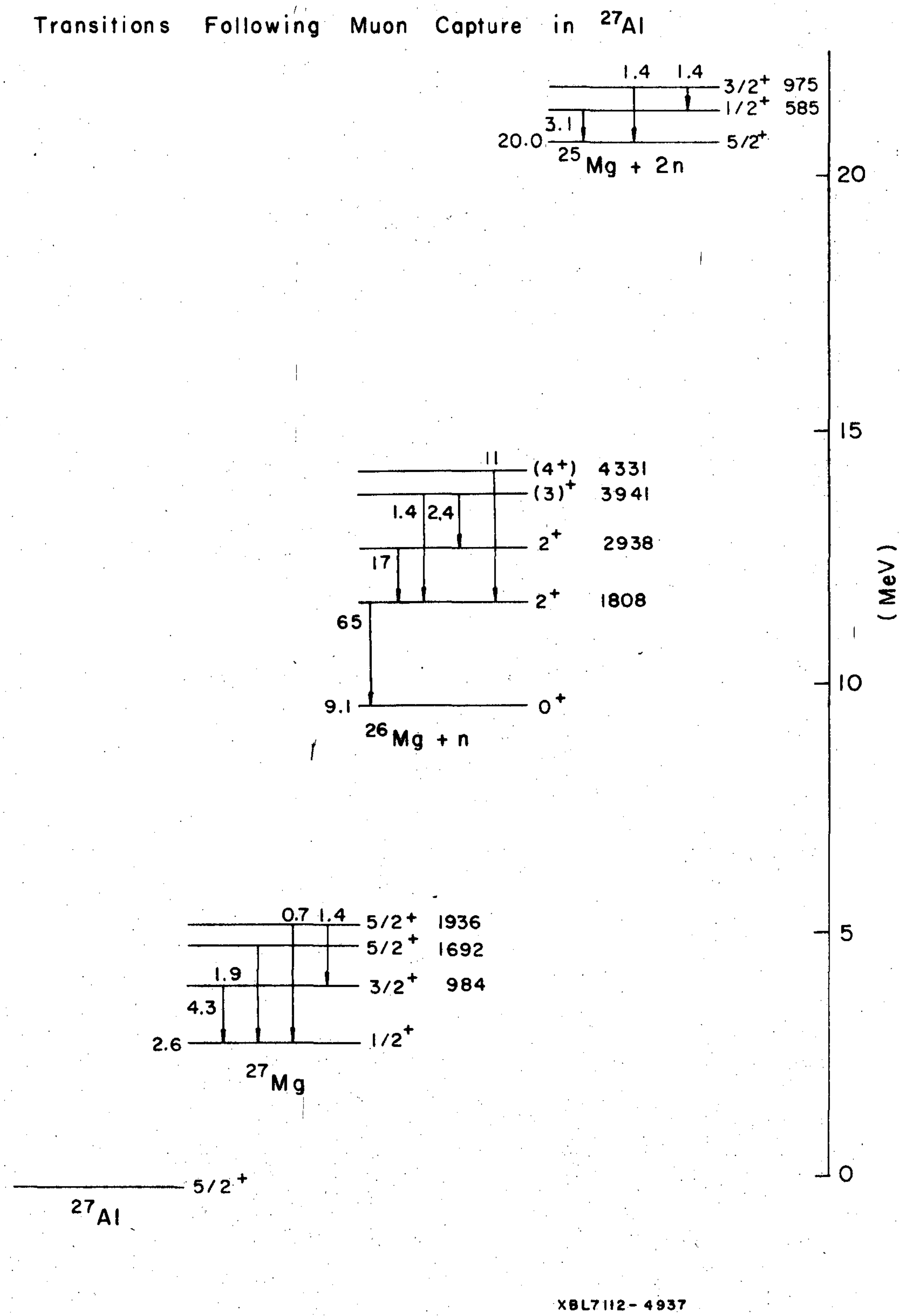

Transitions Following Muon Capture in 27Al
1.4
1.4
3/2+ 975
1/2+ 585
3.1
20.0
5/2+
25Mg + 2n
(4+) 4331
(3)+ 3941
11
1.4
2.4
2+ 2938
17
2+ 1808
65
9.1
0+
26Mg + n
0.7
1.4
5/2+ 1936
5/2+ 1692
1.9
3/2+ 984
4.3
2.6
1/2+
27Mg
5/2+
27Al
20
15
10
5
0
(MeV)
XBL7112-4937

Fig. 5

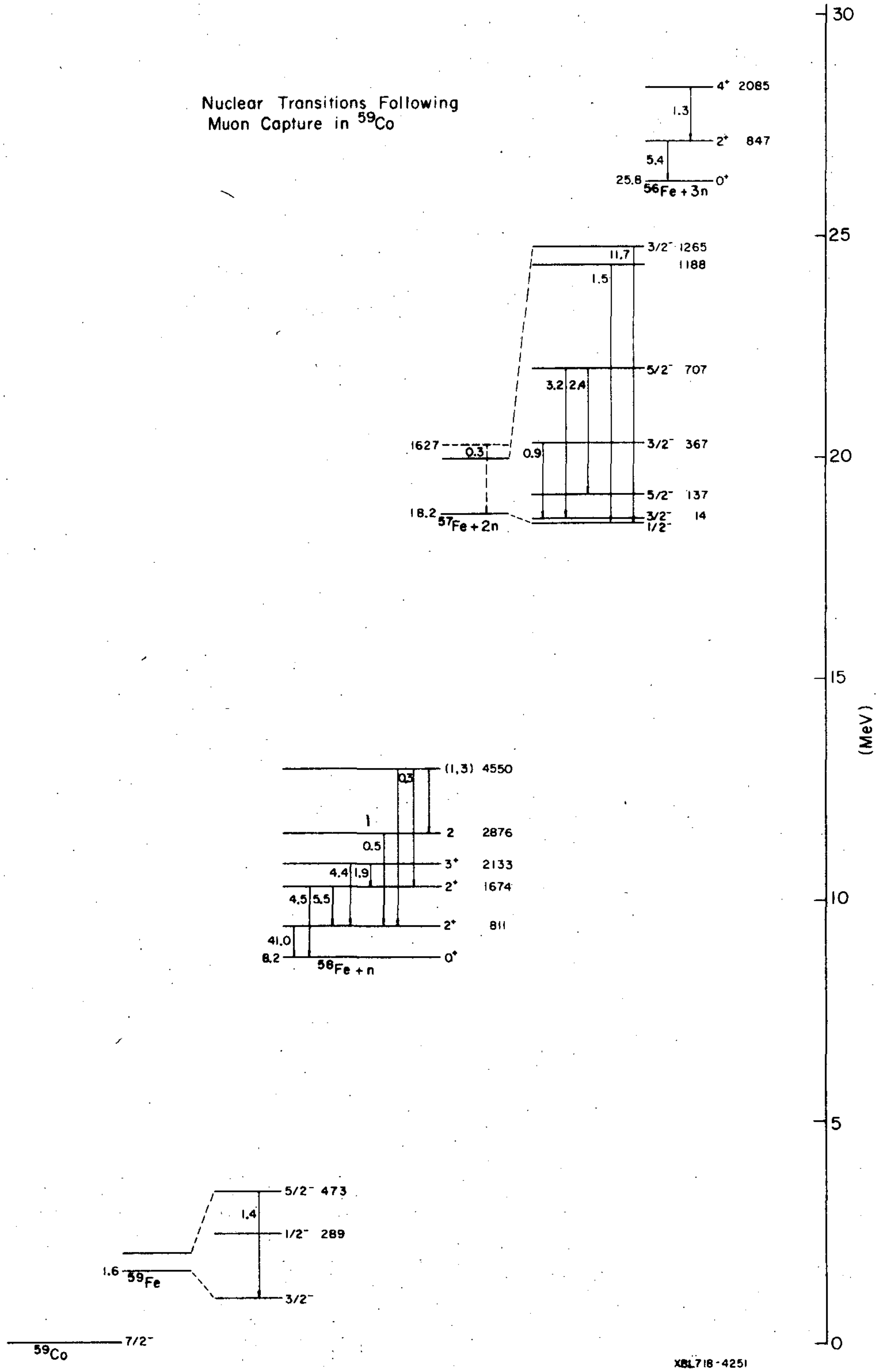
Nuclear Transitions Following Muon Capture in ^{59}Co
4+ 2085
1.3
2+ 847
5.4
25.8 $^{56}Fe + 3n$ 0+
3/2- 1265
11.7
1188
1.5
5/2- 707
3.2 2.4
3/2- 367
1627 0.3
0.9
5/2- 137
18.2 $^{57}Fe + 2n$
3/2- 14
1/2-
(1,3) 4550
0.3
1
2 2876
0.5
3+ 2133
4.4 1.9
2+ 1674
4.5 5.5
2+ 811
41.0
8.2 $^{58}Fe + n$ 0+
5/2- 473
1.4
1/2- 289
1.6 ^{59}Fe
3/2-
^{59}Co 7/2-
30
25
20
15
10
5
0
(MeV)
XBL718-4251

Fig. 6

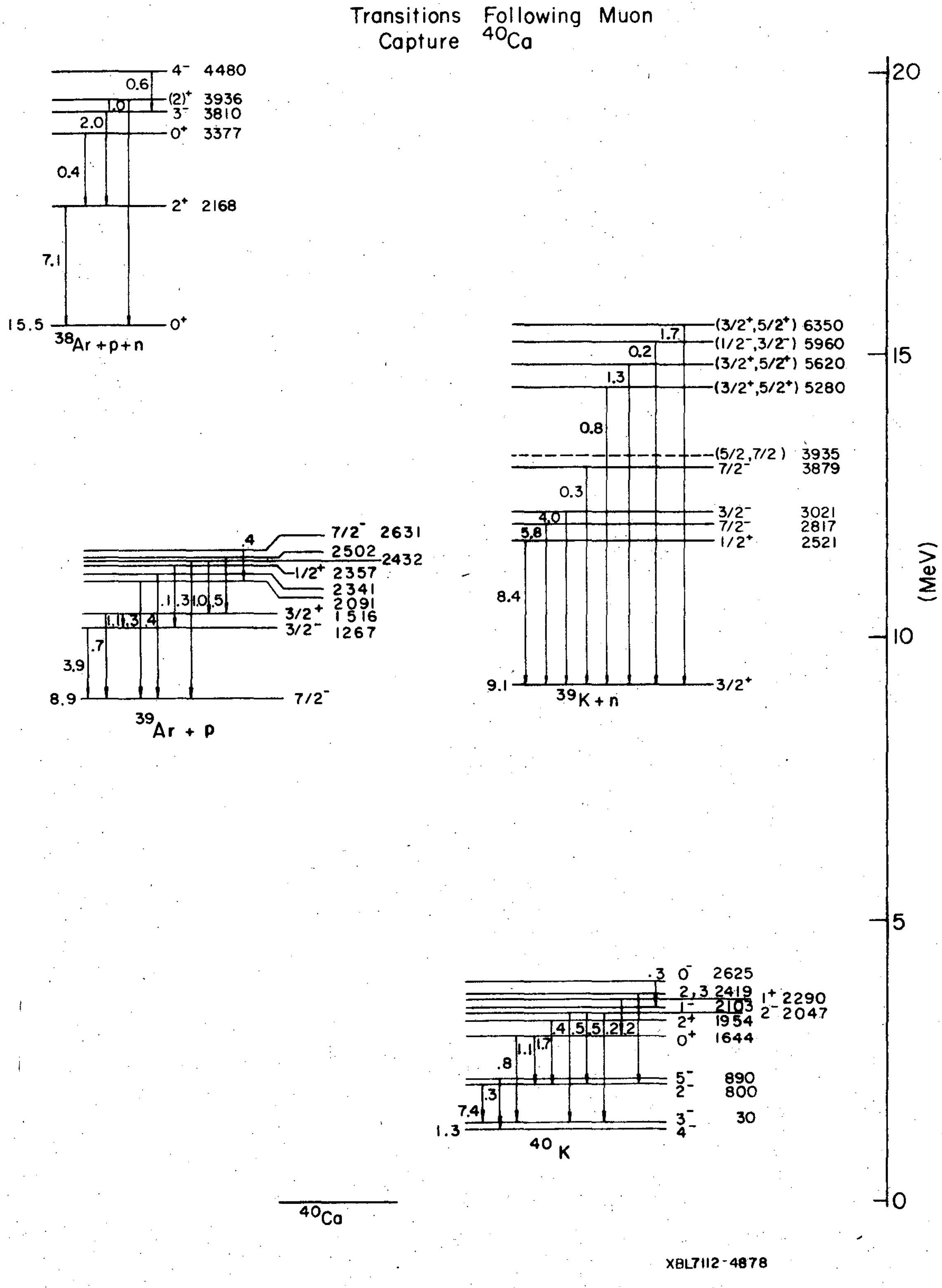

Transitions Following Muon Capture ^{40}Ca
4⁻ 4480
(2)⁺ 3936
3⁻ 3810
0⁺ 3377
2⁺ 2168
0⁺
15.5
^{38}Ar + p + n
7/2⁻ 2631
2502
2432
1/2⁺ 2357
2341
2091
3/2⁺ 1516
3/2⁻ 1267
7/2⁻
8.9
^{39}Ar + p
(3/2⁺,5/2⁺) 6350
(1/2⁻,3/2⁻) 5960
(3/2⁺,5/2⁺) 5620
(3/2⁺,5/2⁺) 5280
(5/2,7/2) 3935
7/2⁻ 3879
3/2⁻ 3021
7/2⁻ 2817
1/2⁺ 2521
3/2⁺
9.1
^{39}K + n
0⁻ 2625
2,3 2419
1⁺ 2290
1⁻ 2103
2⁻ 2047
2⁺ 1954
0⁺ 1644
5⁻ 890
2⁻ 800
3⁻ 30
4⁻
1.3
^{40}K
^{40}Ca
20
15
10
5
0
(MeV)
XBL7112-4878

Fig. 7

γ's/100 μ^- captures	Yield (MeV.mb)	σ_{max} (arb.units)		
1.7	2.0*	29.9	$(3/2^+),5/2^+$	6.35
0.2	1.0	5.5	$(1/2^-,3/2^-)$	5.96
1.3	1.6	19.6	$(3/2^+),5/2^+$	5.62
0.8	3.8*	25.2	$(3/2^+),5/2^+$	5.28
	2.0	1.0		4.93
	2.5*	0.6	$5/2,7/2$	3.94
0.3	1.5*	1.2	$3/2^+,5/2^+$	3.88
2.9	7*	0.8	$3/2^-$	3.02
4.0	15*	16.5	$7/2^-$	2.82
7.1	57	51.0	$1/2^+$	2.53
		65.6	$3/2^+$	
^{40}Ca(μ^-,νn)^{39}K	^{40}Ca($\gamma,p\gamma'$)^{39}K	^{40}Ca(t,α)^{39}K		

^{39}K

XBL 7112-1804

Fig. 8

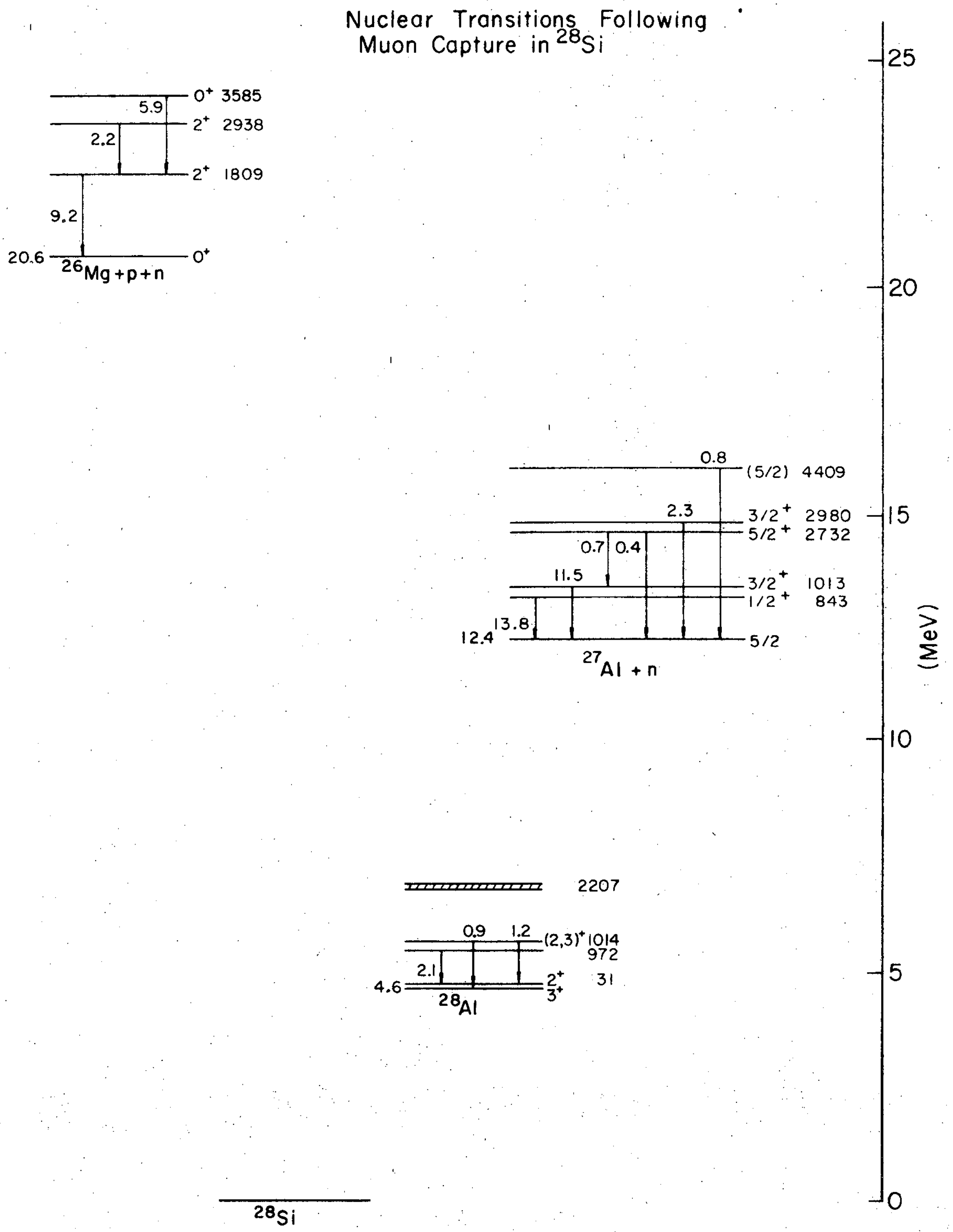
Nuclear Transitions Following Muon Capture in ^{28}Si
0⁺ 3585
5.9
2⁺ 2938
2.2
2⁺ 1809
9.2
20.6
0⁺
^{26}Mg+p+n
0.8
(5/2) 4409
2.3
3/2⁺ 2980
5/2⁺ 2732
0.7
0.4
11.5
3/2⁺ 1013
1/2⁺ 843
13.8
12.4
5/2
^{27}Al + n
2207
0.9
1.2
(2,3)⁺ 1014
972
2.1
2⁺
3⁺
31
4.6
^{28}Al
^{28}Si
25
20
15
10
5
0
(MeV)
XBL7112-4938

Fig. 9

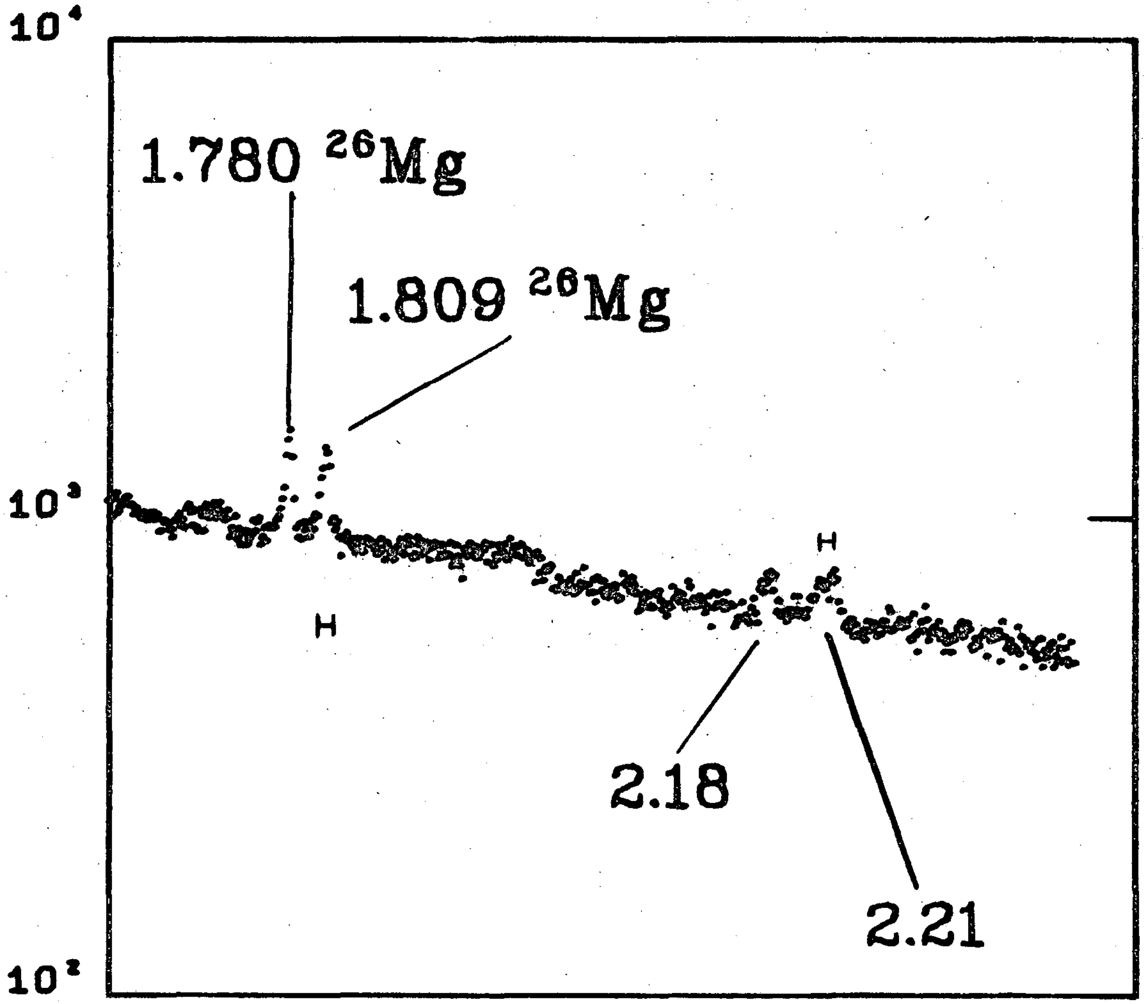

BROAD LINES NEAR 2 MeV
in SILICON TARGET

XBL 719-1341

Fig. 10

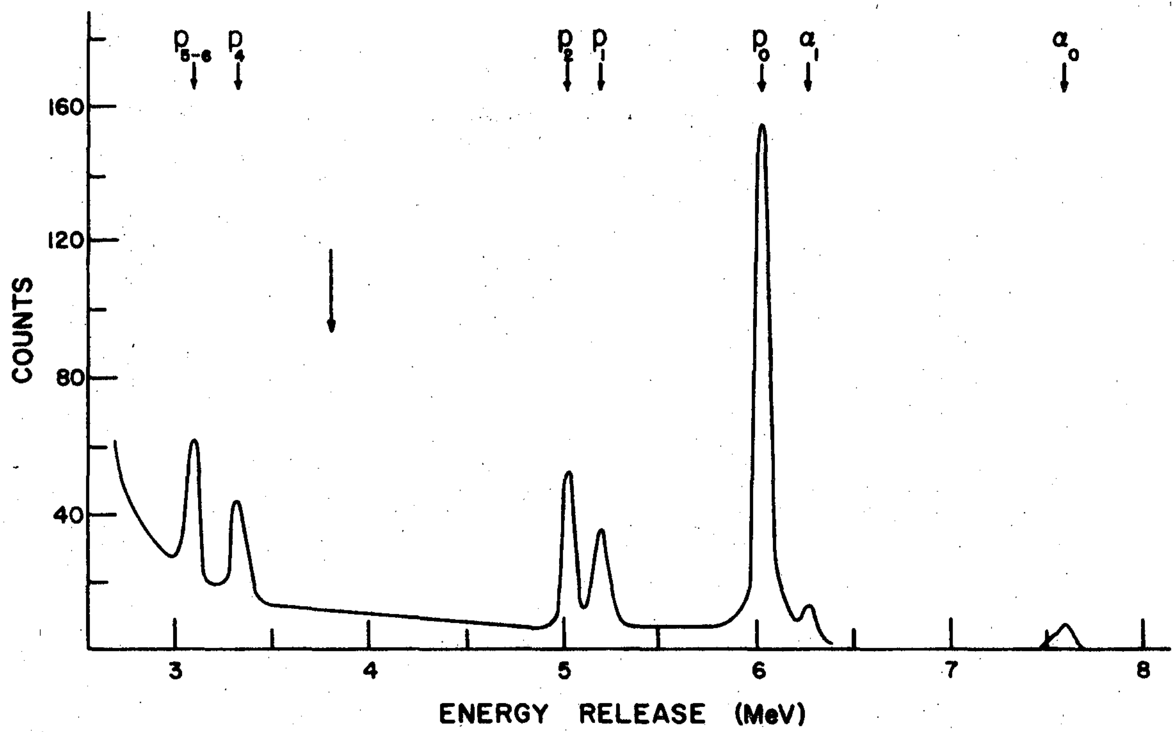

XBL 7112-1805

Fig. 11

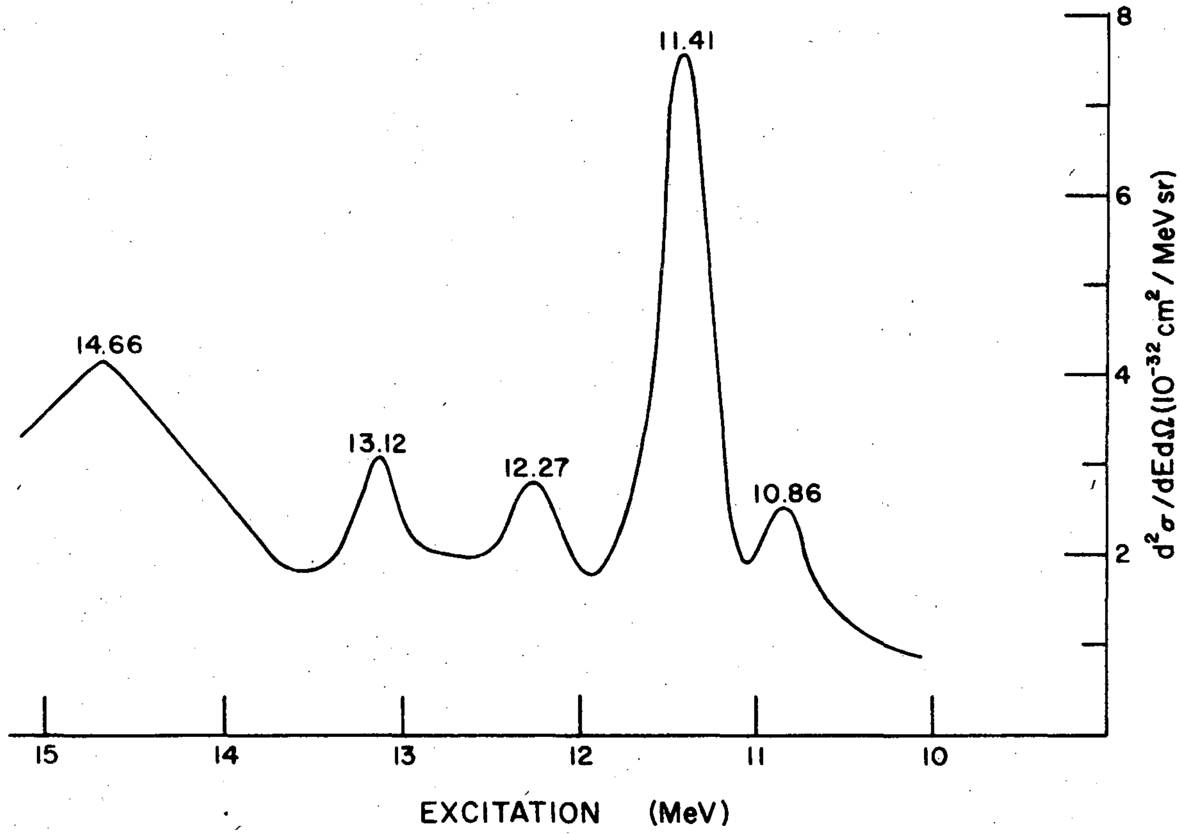

XBL 7112-1806

Fig. 12

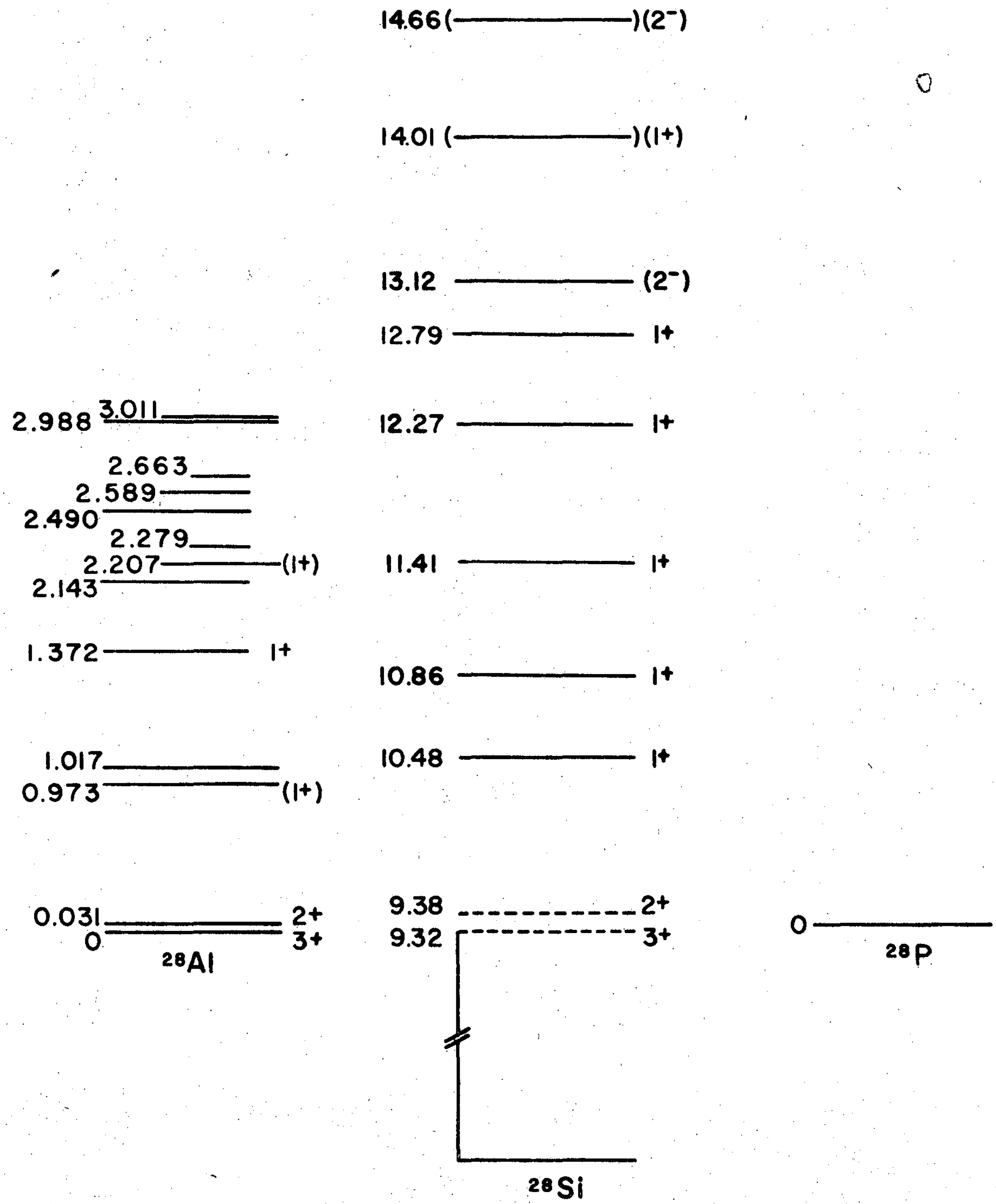

XBL 7112-1807

Fig. 13

Table I. Muon capture in $^{27}Al(5/2^+$ g.s.).

Resultant nucleus	Excited State keV, I^π		Observed γ-ray decay modes		Transition intensities	Population of state	Formation of isotope
^{27}Mg, $1/2^+$	984.1	$3/2^+$	985.5	$3/2^+ \to 1/2^+$	4.3±0.4	2.9±0.5	6.8±0.7
	1692	$5/2^+$	1698.3	$5/2^+ \to 1/2^+$	1.9±0.4	1.9±0.4	
	1936	$5/2^+$	1936.6±1.6	$5/2^+ \to 1/2^+$	0.7±0.4	2.0±0.3	
			956.8±0.4		1.4±0.3		
^{26}Mg, 0^+	1808.9	2^+	1808.0	$2^+ \to 0^+$	65.0±3.0	37.0±4.0	70.0±6.0
	2938.0	2^+	2939.0	$2^+ \to 0^+$	1.4±0.6	19.0±4.0	
			1129.9	$2^+ \to 2^+$	17.1±1.5		
	3940.5	$(3)^+$	1003.8	$(3)^+ \to 2^+$	2.4±0.4	3.8±0.3	
			2130.7	$(3)^+ \to 2^+$	1.4±0.5		
	4331.0	$(4)^+$	2510.5	$(4)^+ \to 2^+$	9.8±0.9	10.7±1.4	
^{25}Mg, $1/2^+$	585.2	$1/2^+$	584.6	$1/2^+ \to 5/2^+$	3.1±0.3	1.7±0.4	4.5±0.5
	974.7	$3/2^+$	975.5	$3/2^+ \to 5/2^+$	1.4±0.3	2.8±0.2	
			390.8	$3/2^+ \to 1/2^+$	1.4±0.2		
						$\Sigma = 81\pm6$	

Table II. Muon capture in ^{59}Co ($7/2^-$ g.s.).

Resultant nucleus	Excited state keV,	I^π	Observed γ-ray decay modes		Transition intensities	Transition intensities, Backenstoss[a]	Population of state	Formation of isotope
^{59}Fe, $3/2^-$	289	$1/2^-$	Below cutoff					
	473	$5/2^-$	472.7	$5/2^- \rightarrow 3/2^-$	1.7±0.3	1.9±0.3	1.7±0.3	1.7±0.3
^{58}Fe, 0^+	810.5	2^+	811.3	$2^+ \rightarrow 0^+$	40.5±4.5	44.0±5.0	30.1±4.6	46.1±5.2
	1674.1	2^+	864.6	$2^+ \rightarrow 2^+$	5.5±0.6	5.1±0.7	8.6±2.1	
			1674.2	$2^+ \rightarrow 0^+$	$4.5^{+0.6}_{-1.2}$	5.0±3.0		
	2133.4	3^+	458.8	$3^+ \rightarrow 2^+$	1.9±0.2	2.2±0.4	6.5±0.9	
			1322.3	$3^+ \rightarrow 2^+$	4.4±0.5			
	2876.0	2	2064	$2 \rightarrow 2^+$	0.5±0.2		$0.2^{+0.5}_{-0.2}$	
	4550	1,3	3743±7	$1,3 \rightarrow 2^+$	0.3±0.3		0.7±0.7	
			2888±8	$1,3 \rightarrow 2^+$	0.3±0.4			
^{57}Fe, $1/2^-$	14.4	$3/2^-$	Below cutoff					18.0±1.4
	136.3	$5/2^-$	Below cutoff			8.0±1.5		
	366.8	$3/2^-$	352.4	$3/2^- \rightarrow 3/2^-$	0.9±0.1	1.2±0.3	1.0±0.1	
	706.4	$5/2^-$	692.5	$5/2^- \rightarrow 3/2^-$	3.2±0.4	3.6±0.7	3.5±0.4	
	1190		1190.4		1.5±0.2		1.5±0.2	
	1265	$3/2^-$	1264.9		11.7±1.3	15.7±2.5	11.7±1.3	
	1627		1627±5		0.3±0.2		0.3±0.2	
^{56}Fe, 0^+	846.75	2^+	847.3	$2^+ \rightarrow 0^+$	5.4±0.6	7.1±1.5	4.1±0.7	5.4±0.8
	2085.1	4^+	1237.8	$4^+ \rightarrow 2^+$	1.3±0.3	2.0±0.7	1.3±0.3	
							Σ = 71±6	

[a]Ref. 7.

Table III. Muon capture in ^{40}Ca.

Resultant nucleus	Excited state keV, I^{π}		Observed γ-ray decay modes		Transition intensities	Transition intensities, Vuilleumier[a]	Population of state	Population of state, Vuilleumier[a]	Population of state, Igo-Kemenes[b]	Formation of isotope
^{40}K, 4^-	30	3^-	Below cutoff							10.5±1.5
	800	2^-	771.3	$2^- \to 3^-$	7.4±0.6	5.87±0.37	5.3±1.1	4.19±0.45	3.62±1.01	
	890	3^-	899.5	$3^- \to 4^-$	0.3±0.3		0.3±0.3			
	1644	0^+	1611	$0^+ \to 3^-$	0.8±0.2	0.89±0.15	1.0±0.3[e]	0.94±0.19		
			841	$0^+ \to 2^-$	1.1±0.2	0.23±0.1				
	1959	2^+	1160[c]	$2^+ \to 2^-$	1.1[d]	0.48±0.1	1.3±0.4	0.56±0.13	0.42±0.17	
	2047	2^-	2010	$2^- \to 3^-$	0.4±0.2	0.38±0.14	1.34±0.12	0.93±0.22	0.45±0.15	
			1251	$2^- \to 2^-$	0.54±0.08					
	2103	1^-	2073	$1^- \to 3^-$	0.5±0.2	0.6±0.1	0.4±0.3	0.36±0.17		
	2290	1^+	643[c]	$1^+ \to 0^+$	0.22±0.10	0.18±0.05	0.35±0.16	0.41±0.13		
	2419	2,3	1620	$2,3 \to 2^-$	0.2±0.2	0.35±0.12	0.2±0.2	0.4±0.2		
	2625	0^-	522[c]	$0^- \to 1^-$	0.29±0.10	0.39±0.1	0.29±0.10	0.29±0.10		
^{39}K, $3/2^+$	2526	$1/2^+$	2521.3	$1/2^+ \to 3/2^+$	7.1±1.8	5.9±0.5	7.1±1.8	5.9±0.5	6.6±0.4	18.1±1.9
	2817	$7/2^-$	2813.5	$7/2^- \to 3/2^+$	4.0±0.5	3.2±0.3	3.8±0.2	3.2±0.3	3.3±0.3	
	3021	$3/2^-$	3018.1	$3/2^- \to 3/2^+$	2.9±0.5	2.1±0.4	2.9±0.5	2.1±0.4	1.6±0.3	
	3879	$7/2^-$	3878.7	$7/2^- \to 3/2^+$	0.3±0.1	0.8±0.5	0.3±0.1	0.8±0.5	0.76±0.2	
	5280	$(3/2^+)5/2^+$	5273±10	$5280 \to 0$	0.8±0.2	0.9±0.6	0.8±0.2	0.9±0.6	0.4±0.2	
	5620	$(3/2^+)5/2^+$	5612±10	$5620 \to 0$	1.3±0.2	0.7±0.5	1.3±0.2	0.7±0.5	0.4±0.2	
	5960	$(1/2^-,3/2^-)$	6000±10	$5960 \to 0$	0.2±0.1		0.2±0.1			
	6350	$(3/2^+)5/2^+$	6335±10	$6350 \to 0$	1.7±0.2	0.8±0.6	1.7±0.2	0.8±0.6		
^{38}K, 3^+	130	0^+	Below cutoff							0.6±0.2
	458	1^+	Not observed			0.28±0.08		0.28±0.08	0.5±0.2	
	1700	1^+	1572	$1^+ \to 0^+$	0.6±0.2	0.54±0.1	0.6±0.2	0.54±0.1	0.9±0.2	
^{39}Ar, $7/2^-$	1267		1266.5	$3/2^- \to 7/2^-$	4.0±0.4	2.8±0.2	1.9±0.9	0.35±0.33	0.99±0.35	6.7±1.3
	1516		1516.5	$3/2^+ \to 7/2^-$	0.7±0.2	1.01±0.14	2.2±0.2	1.99±0.26	2.64±0.56	
			249	$3/2^+ \to 3/2^-$	1.07±0.11	1.17±0.2				
	2091		2091[c]	$2091 \to 0$	0.3±0.2	0.73±0.16	0.0±0.2	0.59±0.19	0.69±0.23	
	2341		2341	$2341 \to 0$	0.4±0.2		0.4±0.2			
	2357	$1/2^+$	1095[c]	$1/2^+ \to 3/2^-$	0.1±0.1	0.38±0.14	0.1±0.1	0.38±0.14	0.53±0.2	
	2432		2432	$2432 \to 0$	0.3±0.2	0.2	1.2±0.8	1.13±0.18	0.76±0.13	
			1166	$2432 \to 1267$	0.9[f]	0.85±0.12				
	2502		984	$2502 \to 1516$	0.5±0.1	0.19±0.1	0.5±0.1	0.19±0.1		
	2631	$7/2^-$	541[f]	$2631 \to 2091$	0.4±0.1	0.2±0.1	0.4±0.1	0.2±0.1		
	3260		Not observed						0.32±0.19	
^{38}Ar, 0^+	2167.7	2^+	2166.6	$2^+ \to 0^+$	7.1±1.1	5.22±0.35	5.2±1.2	3.3±0.4	3.1±0.4	8.5±1.4
	3376.8	0^+	1211.9	$0^+ \to 2^+$	0.4±0.2	0.32±0.08	0.4±0.2	0.32±0.08	0.94±0.16	
	3810.0	3^-	1642.4	$3^- \to 2^+$	2.0±0.4	1.59±0.14	1.3±0.5	0.89±0.22	1.52±0.15	
	3936.1	$(2)^+$	3938.3	$(2)^+ \to 0^+$	1.0±0.3	1.8	1.0±0.3	1.8	1.2±0.3	
	4479.6	4^-	669.9	$4^- \to 3^-$	0.6±0.2	0.7±0.1	0.6±0.2	0.7±0.1		
^{38}Cl, 2^-	1311	4^-	1316	$4^- \to 2^-$	0.4±0.2	0.5±0.1	0.4±0.2	0.5±0.1	1.05±0.17	0.4±0.1
										Σ = 44.8±3.1

[a] Ref. 17.

[b] Ref. 8.

[c] See addendum.

[d] This line is not clearly separable from ^{39}Ar 2432 $\xrightarrow{75\%}$ 1267 transition, with E = 1165 keV. Intensities taken to be consistent with ^{39}Ar 2432 $\xrightarrow{25\%}$ 0 branch.

[e] Population of this state determined from ^{40}K 1644 $\xrightarrow{80\%}$ 30 transition intensity.

[f] See d above.

Table IV. Muon capture in ^{28}Si.

Resultant nucleus	Excited state keV, I^{π}		Observed γ-ray decay modes		Transition intensities	Transition intensities, Pratt[a]	Population of state	Formation of isotope
^{28}Al, 3^+	30.6	2^+	Below cutoff					
	972		942.3	$972 \rightarrow 31$	2.1±0.3		2.1±0.3	4.2±0.6
	1014.5	$(2,3)^+$	1015.1	$1015 \rightarrow 0$	0.8±0.3[b]		2.1±0.5	
			985.7	$1015 \rightarrow 31$	1.2±0.3			
^{27}Al, $5/2^+$	842.9	$1/2^+$	845.0	$1/2^+ \rightarrow 5/2^+$	11.2±1.2	5.0±0.9	13.4±1.2	29.4±2.1
	1013.0	$3/2^+$	1015.1	$3/2^+ \rightarrow 5/2^+$	11.2±1.3[b]	3.6±0.9	11.5±1.3	
	2732	$5/2^+$	2744±2	$5/2^+ \rightarrow 5/2^+$	0.4±0.3		0.8±0.3	
			1720	$5/2^+ \rightarrow 3/2^+$	0.7±0.2			
	2980	$3/2^+$	2989±1	$3/2^+ \rightarrow 5/2^+$	2.3±1.0		2.3±1.0	
	4409	(5/2)	4405	$(5/2) \rightarrow 5/2^+$	0.8±0.1		1.4±0.2	
^{26}Mg, 0^+	1808.9	2^+	1808.2	$2^+ \rightarrow 0^+$	9.2±1.0		1.0±1.6	9.2±1.0
	2938.0	2^+	1129.0	$2^+ \rightarrow 2^+$	2.2±0.4	1.8±1.1	2.2±0.4	
	3584.7	0^+	1779±1	$0^+ \rightarrow 2^+$	6.0±1.2	3.8±1.6	6.0±1.2	
							Σ = 42±3	

[a]Ref. 18.

[b]See text.

TECHNICAL INFORMATION DIVISION
LAWRENCE BERKELEY LABORATORY
UNIVERSITY OF CALIFORNIA
BERKELEY, CALIFORNIA 94720